Transient evolution of weakly nonlinear sloshing waves: an analytical and numerical comparison

DAVID HILL and JANNETTE FRANDSEN[1]
Department of Civil and Environmental Engineering, The Pennsylvania State University, 212 Sackett Building, University Park, PA, 16802, U.S.A. (dfh4@psu.edu); [1]*Department of Civil and Environmental Engineering, Louisiana State University, 3502 CEBA Building, Baton Rouge, LA, 70803, U.S.A. (frandsen@lsu.edu)*

Abstract. The problem of water waves generated in a horizontally oscillating basin is considered, with specific emphasis on the transient evolution of the wave amplitude. A third-order amplitude evolution equation is solved analytically in terms of Jacobian elliptic functions. The solution explicitly determines the maximum amplitude and nonlinear beating period of the resonated wave. An observed bifurcation in the amplitude response is shown to correspond to the elliptic modulus approaching unity and the beating period of the interaction approaching infinity. The theoretical predictions compare favorably to fully nonlinear simulations of the sloshing process. Due to the omission of damping, the consideration of only a single mode, and the weakly nonlinear framework, the analytical solution applies only to finite-depth, non-breaking waves. The inviscid numerical simulations are similarly limited to finite depth.

Key words: evolution equations, nonlinear waves, sloshing waves

1. Introduction

Sloshing waves generated in a rectangular basin have been well studied in the past, theoretically, experimentally, and numerically. Initially, emphasis was placed on determining the steady-state amplitude response. Many of the salient features of steady-state response diagrams, including the effects of nonlinearity, dispersion, and damping, are discussed by Chester [1] and Chester and Bones [2]. Weakly nonlinear inviscid studies of the steady-state response in water of finite depth were carried out by Ockendon and Ockendon [3] and Faltinsen [4]. A thorough review is provided by Ibrahim *et al.* [5].

Some investigations have looked at the transient behavior of the amplitude as well. Of interest are how the transient maximum amplitude compares to the steady-state value and how the nonlinear beating period varies with the parameters of the problem. Lepelletier and Raichlen [6] solved the shallow-water equations numerically and demonstrated good agreement between their calculations and experiments. Representing a different approach, Wu *et al.* [7] used finite elements to investigate three-dimensional sloshing in inviscid rectangular basins of finite depth.

Faltinsen *et al.* [8] developed an infinite-dimensional modal system and then reduced it, through the assumption of small forcing amplitude, in order to apply it to sloshing tanks. The theory was found to agree well with experiments, provided the water was relatively deep. Faltinsen and Timokha [9] extended this work to improve its applicability to shallower water. Their results accurately reproduced transient behavior in shallow experiments as well as reproduced the steady-state response diagrams of Chester and Bones [2]. In addition, discussion
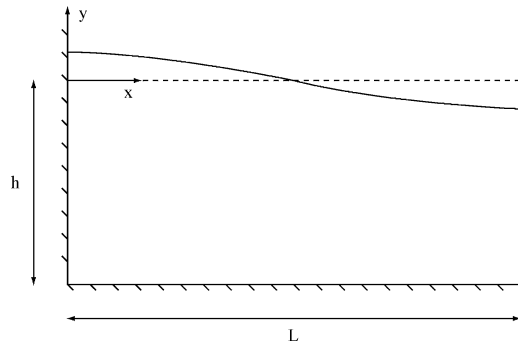
Figure 1. Schematic of basin geometry.

of the dissipation associated with wave breaking was given, with the conclusion that an adequate theory does not yet exist.

An analytical study of the maximum transient amplitude, in the limits of no damping, weak nonlinearity, and finite depth was carried out by Hill [10]. His theoretical predictions showed qualitative agreement with the experiments of Lepelletier and Raichlen [6] and good quantitative agreement with the experiments of Faltinsen *et al.* [8].

The primary contribution of the present paper is to present an analytic solution for the full transient evolution of a finite-depth wave in a basin set into motion from a state of rest. Following the approach of Weiland and Wilhelmsson [11, Chapter 14], a solution to the amplitude evolution equation in terms of Jacobian elliptic functions is obtained. From this solution, the timescale of the nonlinear evolution and the maximum wave amplitude are explicitly determined. From an application point of view, this knowledge is significant. As an example, consider the case of a seismically generated wave in a harbor or fluid-storage container. If the predicted maximum amplitude is large, but the timescale of evolution significantly exceeds the duration of the finite forcing, the wave will never have the opportunity to grow to this maximum value.

The advantage of the present analytic approach is that an extremely compact result is obtained, allowing for rapid and straightforward exploration of a broad range of parameter space. To clarify the scope of the present analysis, however, the weakly nonlinear approach constrains the oscillation amplitude of the basin and therefore the maximum allowable wave steepness. Moreover, the consideration of a single mode and the omission of damping preclude application to shallow water.

To investigate the validity of the analytic solution, it is then compared to fully nonlinear finite-difference simulations of the sloshing process. For a test case in water of finite depth, it is found that the two methodologies yield extremely similar results.

2. Formulation

To begin, consider an inviscid, two-dimensional, first-mode wave of wavenumber k, linear frequency ω, and linear amplitude a in a basin of length L and depth h, as shown in Figure 1. The wavenumber is therefore equal to π/L. The basin is oscillated along the x-axis with an amplitude b and excitation frequency $\omega_e = \omega + \Delta$. The ratio b/L is taken to be much less than unity and is adopted as the expansion parameter ϵ.

The variables of interest are the velocity potential $\Phi(x, y, t)$, which satisfies Laplace's equation, and the free-surface displacement $\eta(x, t)$. The boundary conditions on these variables

include the condition of zero normal velocity, *i.e.,* $\Phi_n = 0$ on all solid boundaries. Note that the 'n' subscript denotes the derivative in the normal direction. The boundary conditions also include the familiar kinematic and dynamic conditions [12, Section 227] imposed at the free surface ($y = \eta(x, t)$). Taylor expanding these conditions to the undisturbed free surface ($y = 0$) and truncating at the third order yields

$$g\eta + \Phi_t = -\frac{1}{2}\nabla\Phi \cdot \nabla\Phi - \eta\Phi_{ty} - \frac{1}{2}\eta^2\Phi_{tyy} - \frac{1}{2}\eta(\nabla\Phi \cdot \nabla\Phi)_y \tag{1}$$

$$\Phi_y - \eta_t = \Phi_x\eta_x - \eta\Phi_{yy} - \frac{1}{2}\eta^2\Phi_{yyy} + \Phi_{xy}\eta\eta_x. \tag{2}$$

The problem is next scaled by adopting the following:

$$(h^*, x^*, y^*) = \frac{(h, x, y)}{L} \quad t^* = t\sqrt{g/L} \quad (\omega^*, \omega_e^*) = \frac{(\omega, \omega_e)}{\sqrt{g/L}}$$

$$\Delta^* = \frac{\Delta}{\epsilon^{2/3}\sqrt{g/L}} \quad a^* = \frac{a}{\epsilon^{1/3}L},$$

where asterisks denote scaled quantities. The asterisks are subsequently dropped and non-dimensional quantities are understood, unless otherwise specified.

Finally, both the free-surface displacement and the velocity potential are taken to be series expansions in the parameter ϵ. For example, the expression for the free-surface displacement is given by

$$\eta = \epsilon^{1/3}\eta_{01}\cos(\pi x)e^{-i\omega_e t} + \epsilon^{2/3}\eta_{10}\cos(2\pi x) + \epsilon^{2/3}\eta_{12}\cos(2\pi x)e^{-2i\omega_e t}$$
$$+ \epsilon\eta_{21}\cos(\pi x)e^{-i\omega_e t} + \epsilon\eta_{23}\cos(3\pi x)e^{-3i\omega_e t} + c.c, \tag{3}$$

where *c.c.* denotes the complex conjugate of the expression.

Solution of this boundary-value problem at successive orders of ϵ is straightforward but lengthy, with full details provided by Hill [10]. The first order yields the linear solution while the second order yields a superharmonic (η_{12}) term and a temporally steady, spatially periodic (η_{10}) term. Finally, at the third order, there is a third-order superharmonic (η_{23}) and a secular forcing term that is in phase with the fundamental harmonic (η_{21}).

In order to guarantee a solution at this third order, a solvability, or orthogonality, condition [13, p. 54] is required in order to remove the secular terms. The application of this solvability condition leads directly to an evolution equation for the wave amplitude,

$$\dot{a} = i\Delta a - i\beta - i\lambda|a|^2 a. \tag{4}$$

Note that the dot notation refers to differentiation with respect to a slow time scale $\tau = \epsilon^{2/3}t$ and that β and λ are, respectively, forcing and depth parameters given by

$$\beta = \frac{2\omega_e}{\pi}\tanh(\pi h), \qquad \lambda = \omega_e\pi^2\frac{\cosh(6\pi h) - 6\cosh(4\pi h) - 15\cosh(2\pi h) - 16}{-8\cosh(6\pi h) + 16\cosh(4\pi h) + 8\cosh(2\pi h) - 16}.$$

The case of $\lambda = 0$ that occurs when $\pi h = 1\cdot 06$ corresponds to the so-called 'critical depth' [14] and the cases of $\lambda \gtrless 0$ correspond to $\pi h \lessgtr 1\cdot 06$. In the vicinity of this critical depth, the scaling adopted above becomes invalid. As shown by Waterhouse [15], a more rigorous re-scaling of the problem yields a result that is uniformly valid for all non-shallow depths. This approach would yield an evolution equation quintic, rather than cubic, in wave amplitude. As this higher-order evolution equation would significantly complicate analytic solution, this re-scaling is not adopted in the present analysis, with the consequence that the obtained solution is not expected to be valid at the critical depth.

Noting that the amplitude a in (4) is complex, it may be represented as a real amplitude and phase, $a = A e^{i\theta}$, yielding the coupled equations

$$\dot{A} = -\beta \sin \theta, \tag{5}$$

$$A\dot{\theta} = -\beta \cos \theta + \Delta A - \lambda A^3. \tag{6}$$

Next, it is straightforward to show that

$$\beta A \cos \theta - \frac{1}{2} \Delta A^2 + \frac{1}{4} \lambda A^4 \equiv \Gamma \tag{7}$$

is a constant of motion. For a basin starting from rest, with the initial condition $A_i = 0$, it is clear that $\Gamma = 0$. As a result, it can be shown from (7) that

$$\cos \theta = \frac{\Delta}{2\beta} A - \frac{\lambda}{4\beta} A^3$$

for all subsequent times. Combining this with (5) leads to

$$\left[\frac{\mathrm{d}}{\mathrm{d}t} (A^2) \right]^2 = -\frac{\lambda^2}{4} \left[(A^2)^4 - \frac{4\Delta}{\lambda} (A^2)^3 + \frac{4\Delta^2}{\lambda^2} (A^2)^2 - \frac{16\beta^2}{\lambda^2} A^2 \right] = f(A^2), \tag{8}$$

where it is noted that the right-hand side is quartic in A^2. In the straightforward extension to non-zero initial conditions ($\Gamma \neq 0$), the polynomial on the right-hand side of (8) would be modified by the presence of Γ.

3. Solution

The solution to this equation is provided by Weiland and Wilhelmsson [11, Chapter 14] and the details depend upon whether $f(A^2) = 0$ has four real roots or two real roots and a complex conjugate pair. It can be shown that the case of four real roots will occur when

$$\Delta \geq \left(\frac{27\lambda\beta^2}{2} \right)^{1/3} \quad \lambda \text{ positive,}$$

$$\Delta \leq \left(\frac{27\lambda\beta^2}{2} \right)^{1/3} \quad \lambda \text{ negative.}$$

It will be seen in Section 4.1 that this corresponds precisely to the bifurcation frequency in the amplitude response diagram.

In this case of four real roots, denote them as $A_d^2 \geq A_c^2 \geq A_b^2 \geq A_a^2$. Next, the change of variables

$$s^2 = \frac{(A_d^2 - A_b^2)(A^2 - A_a^2)}{(A_b^2 - A_a^2)(A_d^2 - A^2)}$$

reduces (8) to

$$(\dot{s})^2 = n^2 (1 - s^2)(1 - m^2 s^2), \tag{9}$$

where the parameters n and m are given by

$$n^2 = \frac{\lambda^2}{16} (A_c^2 - A_a^2)(A_d^2 - A_b^2), \tag{10}$$

$$m^2 = \frac{(A_b^2 - A_a^2)(A_d^2 - A_c^2)}{(A_c^2 - A_a^2)(A_d^2 - A_b^2)}. \tag{11}$$

The solutions for s and, in turn, A are given in terms of the elliptic function sn:

$$s^2 = \text{sn}^2[n(\tau + \tau_0), m], \tag{12}$$

$$A^2 = A_d^2 - \frac{(A_d^2 - A_a^2)(A_d^2 - A_b^2)}{A_d^2 - A_b^2 + (A_b^2 - A_a^2)\text{sn}^2[n(\tau + \tau_0), m]}, \tag{13}$$

where τ_0 is determined by the initial condition on A.

From this solution, it is seen that A oscillates between the minimum amplitude A_a and the maximum amplitude A_b. Significantly, it is also seen that the period of the oscillation, also called the nonlinear interaction period, or the beating period, is explicitly given by

$$T = \frac{2K(m)}{n}, \tag{14}$$

where K is the complete elliptic integral of the first kind. If the basin is starting from rest, which has indeed been assumed, $A_a = 0$ and $\tau_0 = 0$ by definition.

In the case of only two real roots, denote them as $A_b^2 \geq A_a^2$ and represent the complex conjugate pair as $p \pm q\text{i}$. Introducing

$$G_1 = \sqrt{(A_b^2)^2 - 2pA_b^2 + p^2 + q^2}, \qquad G_2 = \sqrt{(A_a^2)^2 - 2pA_a^2 + p^2 + q^2},$$

the solution for A is now given by

$$A^2 = \frac{2(A_b^2 - A_a^2)G_1G_2/(G_1 - G_2)^2}{(2G_2/G_1 - G_2) + 1 - \text{cn}[2n(\tau + \tau_0), m]} + \frac{A_a^2 G_1 - A_b^2 G_2}{G_1 - G_2}. \tag{15}$$

In this instance, the parameters n and m are given by

$$n^2 = G_1 G_2 \frac{\lambda^2}{16}, \tag{16}$$

$$m^2 = \frac{1}{2}\left\{1 - \frac{1}{G_1 G_2}[A_a^2 A_b^2 - p(A_a^2 + A_b^2) + p^2 + q^2]\right\}. \tag{17}$$

As previously, A oscillates between A_a and A_b with a period given by $T = 2K(m)/n$.

4. Results

4.1. GENERAL CHARACTERISTICS

Some of the general features of the amplitude evolution are illustrated in Figure 2, for the case of $\beta = \lambda = 1$. Given that $\lambda > 0$ in this case, the water depth is less than the critical value. Figure 2(a) shows the temporal evolution of the wave amplitude for three representative values of the detuning parameter Δ. It is clear that both the maximum amplitude A_b and the beating period T are strong functions of Δ. Moreover, both A_b and T *initially* increase with increasing Δ. At larger values of Δ, however, both A_b and T are seen to dramatically decrease, suggesting the present of a bifurcation point somewhere in the range of $2 < \Delta < 4$. Hill [10] showed that this bifurcation point was given by

$$\Delta = \left(\frac{27\lambda\beta^2}{2}\right)^{1/3}. \tag{18}$$

As this bifurcation point is approached, the interaction period of the response approaches infinity. Mathematically, this corresponds to the elliptic modulus m approaching unity, which
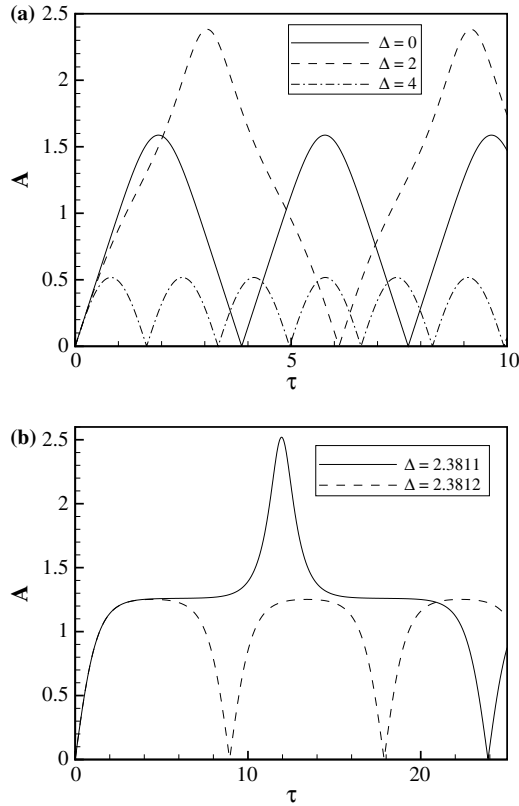
Figure 2. (a) Temporal evolution of wave amplitude A for the cases $\Delta = 0$, 2, 4; $\beta = \lambda = 1$. (b) Temporal evolution of wave amplitude for the cases $\Delta = 2.3811$, 2.3812 (values bracketing the bifurcation point); $\beta = \lambda = 1$.
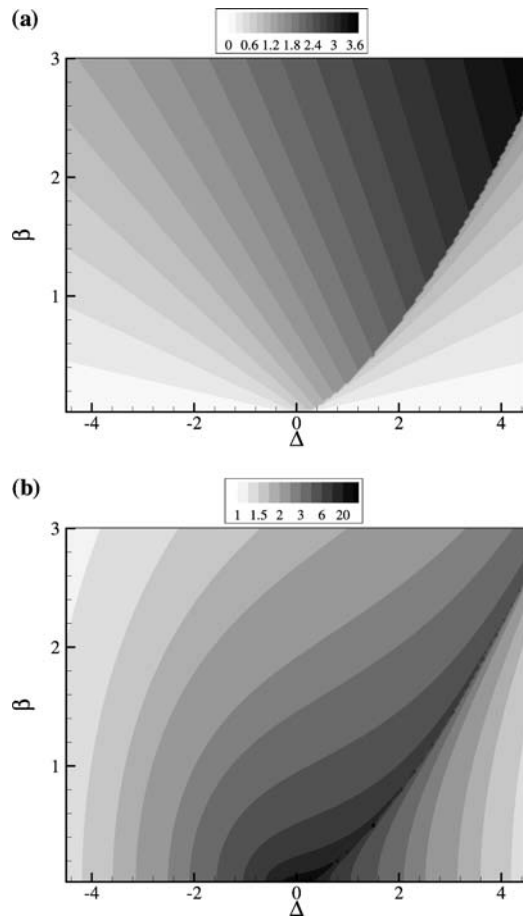

Figure 3. (a) Contours of maximum amplitude A_b as a function of β and Δ for $\lambda = 1$. (b) Contours of beat period T as a function of β and Δ for $\lambda = 1$.

replaces the sn and cn functions with the hyperbolic tanh and sech functions. Additionally, at this point, the amplitude 'jumps' between the values $(8\Delta/3\lambda)^{1/2}$ and $(2\Delta/3\lambda)^{1/2}$. This sharp change in amplitude response is clearly shown in Figure 2(b), which shows the temporal evolution of the wave amplitude at two values of Δ narrowly bracketing the bifurcation value.

Further increases in Δ lead to steady decreases in the maximum amplitude and period. This is the classic hard-spring Duffing-type response that has been extensively demonstrated for steady-state [3,4] and transient [6,10] sloshing waves. Had λ been negative in this example, the response would have followed that of a soft-spring oscillator instead.

Figure 3 shows contours of the maximum amplitude A_b and beat period T in (Δ, β) parameter space, for the case of $\lambda = 1$. In both instances, the curve, or bifurcation 'line,' given by (18) is clearly evident. The results that were shown in Figure 2 ($\beta = 1$, variable Δ) are therefore just a subset of the information shown in Figure 3. This can be seen by scanning horizontally in Figure 3(a) at the value $\beta = 1$. A slow steady increase in A_b with increasing Δ
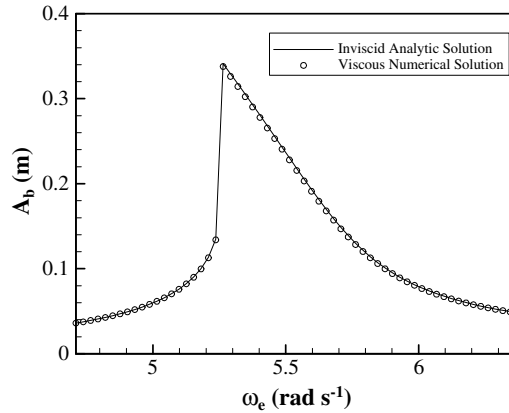
Figure 4. Dimensional response diagrams for the maximum amplitude A_b, as predicted by the present inviscid analytical solution and the viscous numerically-integrated solution of Hill [10]. The dimensional parameters are $h = L = 1\,\text{m}$, $b = 0.005\,\text{m}$, $\nu = 10^{-6}\,\text{m}^2\,\text{s}^{-1}$.

is initially observed. At the bifurcation frequency, there is a dramatic drop in response, followed by further decreases in A_b with increasing Δ.

What is *new* in this figure is information about how A_b and T vary with changes in β. The effect of the forcing parameter on the maximum response is fairly straightforward. It is observed that A_b increases monotonically and smoothly with increasing β for $\Delta < 0$. For the case of $\Delta > 0$, the increase in A_b is again monotonic with increasing β, but a bifurcation, or finite upwards jump, is observed. The effect of changes in β on the beat period is more complex. For $\Delta < 0$, there is a slight monotonic decrease in T with increasing β. For $\Delta > 0$, however, the beat period initially asymptotically increases towards infinity as the bifurcation point is approached. Further increases in β lead to monotonic decreases in T.

Before moving on to consider comparisons between the weakly nonlinear perturbation solution and fully nonlinear numerical simulations, it is worth remarking upon the omission of damping from the present solution. For any non-zero fluid viscosity, the wave amplitude will tend towards a steady-state value, rather than oscillate in the manner shown in Figure 2. However, for a weakly viscous wave in a non-shallow basin, the amplitude does so extremely slowly [8]. For a basin set into motion from a state of rest, therefore, the difference in the global maximum amplitudes as predicted by viscous and inviscid theories is extremely small. To show this, a comparison will be made between the analytic solutions of (13) and (15) and numerical integration of the damped version of the evolution equation given by Hill [10].

Specifically, consider the dimensional example of water waves (kinematic viscosity $\nu = 10^{-6}\,\text{m}^2\,\text{s}^{-1}$) in a basin having great breadth and a length and depth of 1 m. Forcing frequencies in the band of 85–115% of the natural frequency of $5.541\,\text{rad\,s}^{-1}$ are considered. In all cases, the forcing amplitude is $0.5\,\text{cm}$. As shown in Figure 4, the resulting viscous and inviscid transient amplitude response diagrams are nearly indistinguishable. The maximum percent difference between the two curves is 1.2%.

Additional support for the conclusion that damping is relatively unimportant for weakly viscous waves in non-shallow basins comes from Wu *et al.* [16], who consider damping in basins in the linear limit. They define a Reynolds number as (dimensional variables)
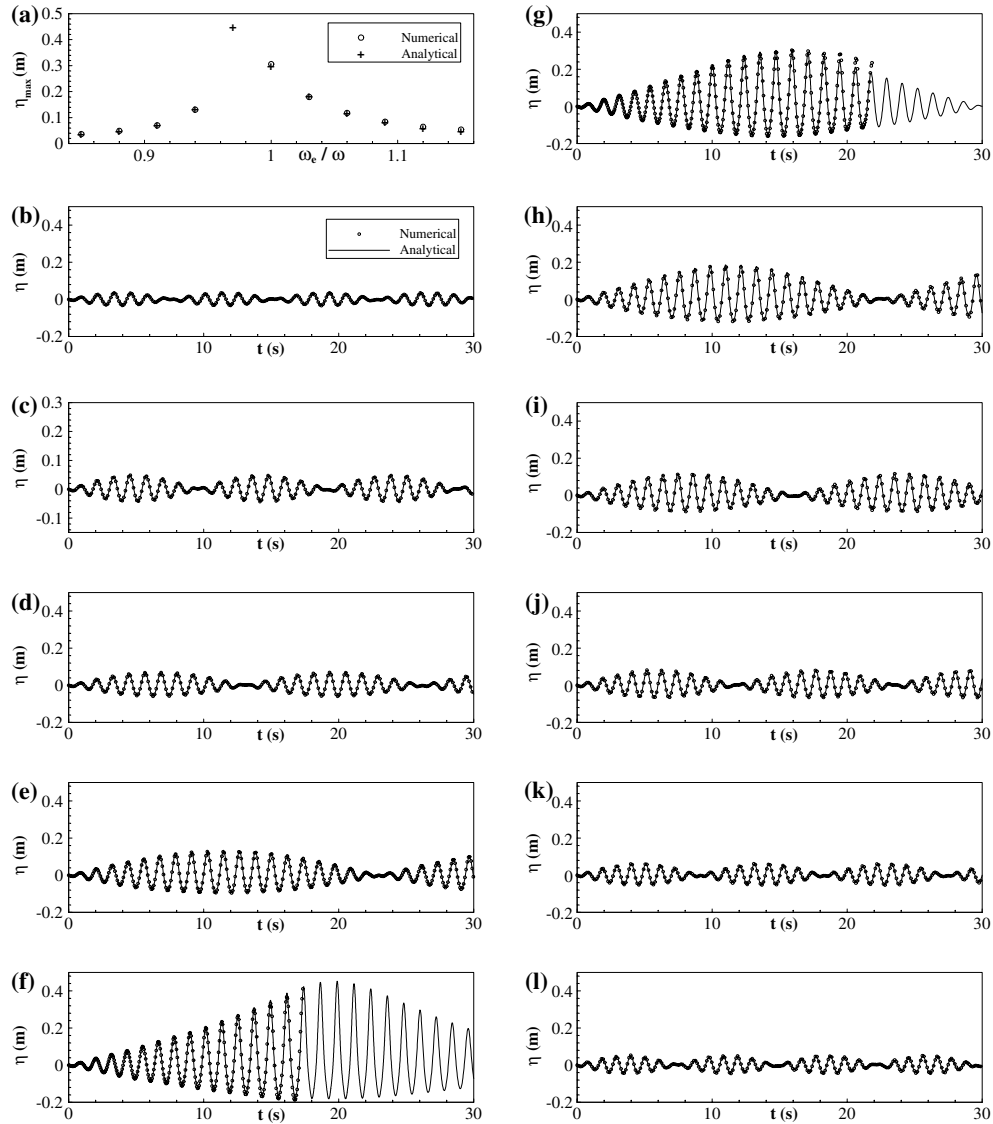
$$\text{Re} = \frac{h\sqrt{gh}}{\nu},$$

Figure 5. (a) Analytical (+) and numerical (○) response diagrams for maximum end-wall free-surface elevation; $h = L = 1$ m, $b = 0.005$ m. (b)–(l) analytical calculations (−) and numerical (○) simulations of the transient end-wall free-surface elevation, $h = L = 1$ m, $b = 0.005$ m. Subplots (b)–(l) correspond to $\omega_e/\omega = 0.85, 0.88, 0.91, 0.94, 0.97, 1.00, 1.03, 1.06, 1.09, 1.12, 1.15$.

and their calculations show that, for Reynolds numbers on the order of 10^3, the damping effects become quite slight. Given that, for the present calculations, the Reynolds number is on the order of 10^6, the omission of damping does indeed seem justified.

4.2. Comparison with numerical simulations

Experimental investigations suitable for comparison to the present theory are scarce. One of the problems is that most existing studies [2, 6, 17] were carried out with shallow basins. As is well-known and as discussed at length by Faltinsen and Timokha [9], shallow water presents a problem in that the higher modes are internally resonant rather than being bound Stokes waves. In this case, solvability requires an evolution equation for each mode, resulting in a

coupled set. While analytic solution of this set remains possible for a low number of modes (see Mei and Unluata [18, pp. 181–202], for the progressive-wave, two-harmonics solution), numerical integration becomes the solution method of choice for larger sets. Application of the present theory, which only derives an amplitude equation for the fundamental mode, to the case of shallow water will result in severe over-estimation of the maximum amplitudes, as shown by Hill [10].

A second problem is that most existing studies [2,19,17] present response diagrams for the steady-state amplitudes and give no information about the transient amplitudes or the non-linear beat period. Notable exceptions include the works of Lepelletier and Raichlen [6] and Faltinsen *et al.* [8]. Precluding precise comparisons with these last two studies, however, are the facts that the former experiments were conducted for quite shallow basins and that the latter experiments were conducted with initially non-quiescent free surfaces.

Therefore, in order to assess the performance of the present analytical solution, it will be compared with numerical simulations of the sloshing process. The two-dimensional simulations are carried out with a fully nonlinear finite-difference potential-flow solver. As discussed in the previous section, the omission of viscosity is justified for large basins. The equations and boundary conditions are the same as given in Section 2 with the significant exception that the free-surface boundary conditions are utilized in their fully nonlinear forms, rather than in the weakly nonlinear forms demanded by the analytical solution.

The equations are discretized using a second-order Adams–Bashforth scheme. A modified σ transformation is used to map the liquid domain onto a rectangle, such that the moving free surface in the physical plane is mapped to a fixed line in the computational domain. In this way, the re-meshing ordinarily required by a moving free surface is avoided. Additionally, this formulation avoids the need to calculate the free-surface velocity components explicitly. The numerical model is limited to non-breaking waves and is valid for any water depth except for shallow water, where viscous effects would become important. A complete description of the numerical model is provided by Frandsen [20].

By use of the same dimensional parameters as given in Section 4.1, the transient evolution of the free-surface elevation η at the tank end-wall was computed from the present weakly nonlinear analytical solution and the fully nonlinear numerical simulation just described. Comparisons were made for 11 forcing frequencies in the range of 85–115% of the natural frequency ω. Note that, in the case of the analytical results, the free-surface elevation was derived from the wave amplitude involving the second- and third-order Stokes wave solutions [14]. For most of the numerical simulations, a 40×80 spatial grid was used, with a time step of 0·003 s. For the most resonant case, a refined grid of 80×120 and a refined time step of 0·0015 s were used.

As shown in Figure 5(b–l), the agreement between the weakly and the fully nonlinear results is generally excellent, both in terms of wave amplitude and beat period. Cases (b) and (l) are the furthest away from resonance and the responses in these cases are very nearly linear. This is evidenced by the small observed elevations, the symmetry between crest and trough, and beat periods which are very close to the linear prediction of $2\pi/|\Delta| = 7.56$ s. Cases (e) and (i) are more resonant and begin to display nonlinearity in the form of asymmetry between crest and trough and, more prominently, in the beat period. Whereas the linear prediction in cases (e) and (i) is 18·90 s, the nonlinear results are 23 and 16 s, respectively.

For the maximum-response case at $\omega_e/\omega = 0.97$ (case (f)), the numerical simulation fails due to excessive wave steepness, $ka \sim 1$. Up until the point of failure, however, the analytical and numerical predictions are in agreement. The one noticeable discrepancy between the analytical and numerical results is demonstrated in case (g). Up to the point of maximum
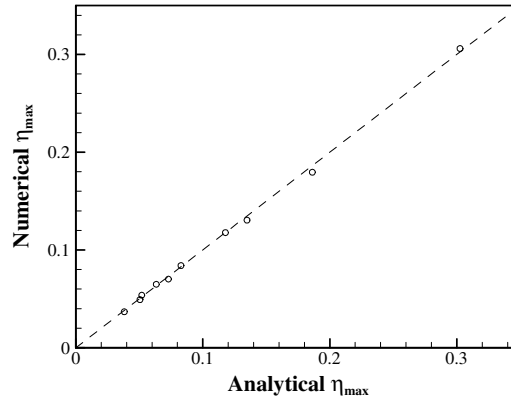
Figure 6. Analytical and numerical values of maximum end-wall free-surface elevation plotted against each other; $h = L = 1$, $b = 0.005$ m. The dashed line corresponds to perfect agreement. Individual points correspond to the different values of excitation frequency ω_e detailed in Figure 5 (b–l).

response, the two methodologies are in agreement. Past the point of the maximum response, the two solutions continue to predict similar trough elevations, but the numerical solution yields higher crest elevations than the analytical solution. For the two cases (f) and (g), it is anticipated that the numerical difficulty could be resolved in part by adding free-surface smoothing, as discussed by Longuet-Higgins and Cokelet [21] and Dold [22].

For both methodologies, values of maximum free-surface elevation (η_{max}) were then extracted and plotted against relative forcing frequency (ω_e/ω) in Figure 5(a) to form maximum-elevation response diagrams. The close overlap of the symbols (numerical – o; analytical – +) from the numerical and the analytical results again confirms the good agreement between the two methodologies. The lack of a numerical data point at $\omega/\omega_e = 0.97$ is due to the numerical difficulty discussed above.

An alternative way to visualize this agreement is presented in Figure 6. This figure was created with the pairs of numerical and analytical η_{max} values that were extracted from Figure 5(b–l). The two values from each pair were plotted against each other, with the numerical value on the vertical axis and the analytical value on the horizontal axis. If the two methodologies were in *exact* agreement, all of the symbols would fall on the line passing through the origin with a slope of 1. As the figure shows, there are deviations from this line of perfect agreement, but they are limited to only a few percent.

5. Concluding remarks

In summary, an analytic solution for the transient development of inviscid sloshing waves in horizontally oscillating rectangular tanks has been presented. The solution is based upon a third-order amplitude equation, previously obtained, for the fundamental mode and is given in terms of Jacobian elliptic functions. The analytic solution thereby explicitly determines the maximum transient amplitude and the nonlinear beat period of the resonated wave. In addition to depending upon the forcing amplitude and frequency, the response of the basin is found to be a function of its relative depth.

There is a bifurcation point in the response, which is easily derived. At this point, the response amplitude is found to jump between two values that differ by a factor of two. Additionally, as the bifurcation point is approached, the beat period tends to infinity. Mathemat-

ically, this corresponds to the elliptic functions governing the response tending to hyperbolic functions instead.

The analytic theory was compared to fully nonlinear finite-difference simulations of the sloshing process. For a finite-depth test case, the agreement between the two methodologies was found to be very good over a wide range of forcing frequencies. At frequencies very close to resonance, the numerical simulations failed, precluding comparisons at those values.

The omission of viscosity in both the analytical and the numerical approaches has been justified for relatively large tanks, where damping is relatively unimportant. In addition to this limitation, the analytical theory is inappropriate for shallow water since it developed an amplitude equation for only the fundamental mode. Consideration of coupled evolution equations for several modes will extend the range of applicability of the perturbation solution.

Finally, there are several attractive future extensions of this work. Three-dimensional effects will obviously appear for more complex basins and/or more complex forcing patterns. For the present case of forcing aligned with an axis of a rectangular basin, three-dimensional waves can not be generated directly by the oscillating tank walls. This is a principle of symmetry similar to the explanation [19] of why, in the two-dimensional case, only waves with odd mode numbers are allowed. However, once large two-dimensional waves have been resonated, it is possible that higher-order interactions can lead to the growth of three-dimensional modes. Additional work of interest includes the effects of random forcing on the response. Repetto and Galletta [23] recently studied the effects on narrow-banded forcing on Faraday resonance and found that the response diagram widened and decreased in amplitude as the forcing bandwidth increased.

References

1. W. Chester, Resonant oscillations of water waves, part 1, theory. *Proc. R. Soc London (A)* 306 (1968) 5–22.
2. W. Chester and J. Bones, Resonant oscillations of water waves, part II, experiment. *Proc. R. Soc. London (A)* 306 (1986) 23–39.
3. J. Ockendon and H. Ockendon, Resonant surface waves. *J. Fluid Mech.* 59 (1973) 397–413.
4. O. Faltinsen, A nonlinear theory of sloshing in rectangular tankes. *J. Ship Res.* 18 (1974) 224–241.
5. R. Ibrahim, V. Pilipchuk and T. Ikeda, Recent advances in liquid sloshing dynamics. *Appl. Mech. Rev.* 54 (2001) 133–199.
6. T. Lepelletier and F. Raichlen, Nonlinear oscillations in rectangle tanks. *J. Engng. Mech.* 114 (1988) 1–23.
7. G. Wu, Q. Ma and R. Eatock Taylor, Numerical simulation of sloshing waves in a 3D tank based on a finite element method. *Appl. Ocean Res.* 20 (1998) 337–355.
8. O. Faltinsen, O. Rognebakke, I. Lukovsky and A. Timokha, Multidimensional model analysis of nonlinear sloshing in a rectangular tank with finite water depth. *J. Fluid Mech.* 407 (2000) 201–234.
9. O. Faltinsen and A. Timokha, Asymptotic model approximation of nonlinear resonant sloshing and in a rectangular tank with small fluid depth. *J. Fluid Mech.* 470 (2002) 319–357.
10. D. Hill. Transient and steady-state amplitudes of forced waves in rectangular basins. *Phys. Fluids* 15 (2003) 1576–1587.
11. J. Weiland and H. Wilhelmsson, *Coherent Non-Linear Interaction of Waves in Plasmas*. New York: Pergamon Press (1977) 353 pp.
12. H. Lamb, *Hydrodynamics*. (Sixth edition) New York: Dover (1932) 738 pp.
13. C. Mei, *The Applied Dynamics of Ocean Surface Waves*. Volume 1 of Advanced Series on Ocean Engineering. Singapore: World Scientific (1989).
14. I. Tadjbakhsh and J. Keller, Standing surface waves of finite amplitude. *J. Fluid Mech.* 8 (1960) 442–451.
15. D. Waterhouse, Resonant sloshing near a critical depth. *J. Fluid Mech.* 281 (1994) 313–318.
16. G. Wu, R. Eatock Taylor and D. Greeves, The effect of viscosity on the transient free-surface waves in a two-dimensional tank. *J. Engng. Mech.* 124 (1998) 77–90.

17. D. Reed J. Yu, H. Yeh and S. Gardarsson, Investigation of tuned liquid dampers under large amplitude excitation. *J. Engng. Mech.* 124 (1998) 405–413.

18. C. Mei and U. Unluata, Harmonic generation in shallow water waves. In: R. Meyer (ed.). *Waves on Beaches and Resulting Sediment Transport*. New York: Academic Press (1972) 462 pp.

19. Z. Feng, Transition to traveling waves from standing waves in a rectangular container subjected to horizontal excitations. *Phys. Rev. Lett.* 79 (1997) 415–418.

20. J. Frandsen, Sloshing motion in exited tanks. *J. Comp. Phys.* 196 (2004) 53–87.

21. M. Longuet-Higgins and E. Cokelet, The deformation of steep surface waves on water i: a numerical method of computation. *Proc. R. Soc. London A* 350 (1976) 1–26.

22. J. Dold, An efficient surface integral algorithm applied to unsteady gravity waves. *J. Comp. Phys.* 103 (1992) 90–115.

23. R. Repetto and V. Galletta, Finite amplitude Faraday waves induced by a random forcing. *Phys. Fluids* 14 (2002) 4284–4289.